

CPP

Contributions to Plasma Physics

www.cpp-journal.org

Editors:

M. Bonitz, Kiel (Editor-in-Chief)
T. Klinger, Greifswald
K.-H. Spatschek, Düsseldorf

Associate Editors:

C. Franck
E. Kovacevic
A. v. Keudell

Managing Editors

D. Naujoks

Coordinating Editor

M. Dewitz

WILEY-VCH

REPRINT

Dynamical Screening and Wake Effects in Classical, Quantum, and Ultrarelativistic Plasmas

Zh. A. Moldabekov^{1,2}, P. Ludwig^{1*}, J.-P. Joost¹, M. Bonitz¹, and T. S. Ramazanov²

¹ Institut für Theoretische Physik und Astrophysik, Christian-Albrechts-Universität zu Kiel, Leibnizstraße 15, 24098 Kiel, Germany

² Institute for Experimental and Theoretical Physics, Al-Farabi Kazakh National University, 71 Al-Farabi str., 050040 Almaty, Kazakhstan

Received 14 November 2014, accepted 20 November 2014

Published online 23 January 2015

Key words Dynamical screening, plasma wakes, complex plasma, quantum plasma, quark-gluon plasma.

Wakefields are of omnipresent nature in non-equilibrium situations, but their appearance and parametrical scaling is very diverse. Therefore, in this work the topological structure and characteristics of the dynamically screened potential is outlined for three representative systems in completely different physical regimes: (i) a classical complex (dusty) plasma, (ii) a degenerate electron-ion plasma at high densities, and (iii) an ultrarelativistic quark-gluon plasma.

© 2015 WILEY-VCH Verlag GmbH & Co. KGaA, Weinheim

1 Introduction

In recent years, wake effects have been extensively studied in classical dusty (complex) plasmas which are popular among experimentalists as an easy to handle reference system for studying strong correlation effects and self-organization in confined and unconfined open systems in non-equilibrium, see e.g. [1–4] and references therein. Therefore, it is very appealing to compare the features of plasma wakes observed in dusty plasmas with those in non-classical plasmas, where the experimental investigation requires sophisticated devices and is not as straightforward as in dusty plasmas. Analogies, but also identified differences may be of direct importance for various fields, where a deviation from the static Yukawa potential due to streaming effects can be expected. Examples include dense plasmas in warm dense matter and condensed matter physics, ion beam physics [5–12] as well as hot electron-positron and *quark-gluon plasmas* (QGP) [13–17].

Considering a stationary non-equilibrium plasma, in the framework of which a charged particle's streaming velocity is constant and defined as an external parameter, the effective *dynamically screened potential* (DSP) is given by [12]:

$$\Phi(\mathbf{r}) = \int d^3\mathbf{k} \frac{Q}{2\pi^2 k^2 \epsilon_L(\mathbf{k}, \mathbf{k} \cdot \mathbf{u})} e^{i\mathbf{k} \cdot \mathbf{r}}, \quad (1)$$

where Q denotes the point-like charge around which the potential distribution is considered, $\epsilon_L(\mathbf{k}, \mathbf{k} \cdot \mathbf{u})$ is the longitudinal dielectric function, and \mathbf{u} is the streaming velocity. In order to compare the dynamical screening of a highly charged dust grain in the classical plasma of gas discharge, an ion in a dense quantum plasma of electrons, and a swift parton in the QGP, the corresponding dielectric functions $\epsilon_L(\mathbf{k}, \mathbf{k} \cdot \mathbf{u})$ are given and appropriate streaming parameters (Mach numbers) are defined in section 2. In the main part, section 3, the topologies and characteristics of the DSPs of the systems under consideration are analysed with respect to different values of the streaming parameter and collisionality of the plasma. For the efficient high resolution computation of the 3D plasma potential in linear response description, KIELSTREAM, a recently developed C++ program is utilized [18].

* Corresponding author. Email: ludwig@theo-physik.uni-kiel.de

2 Ansatz

Within the considered linear response approach, the characteristics of the plasma are modeled by an appropriate dynamic dielectric function.

2.1 Classical dielectric function

The classical dusty plasma is represented by a longitudinal dielectric function which includes a directed ion flow \mathbf{u}_i and a *Bhatnagar-Gross-Krook* (BGK)-type approximation for the ion-neutral collisions [18–20]

$$\epsilon(\mathbf{k}, \omega) = 1 + \frac{1}{k^2 \lambda_{De}^2} + \frac{1}{k^2 \lambda_{Di}^2} \left[\frac{1 + \zeta_i Z(\zeta_i)}{1 + \frac{i\nu_i}{\sqrt{2}k v_{Ti}} Z(\zeta_i)} \right]. \quad (2)$$

Here, we use the electron (ion) Debye length $\lambda_{De(i)} = (\epsilon_0 k_B T_{e(i)} / Q_{e(i)}^2 \bar{n}_{e(i)})^{1/2}$, the ion collision frequency ν_i , the ion thermal velocity $v_{Ti} = (k_B T_i / m_i)^{1/2}$, the substitution $\zeta_i = (\mathbf{k} \cdot \mathbf{u}_i + i\nu_i) / (\sqrt{2}k v_{Ti})$, and the plasma dispersion function $Z(z) = i\sqrt{\pi} \exp(-z^2) \operatorname{erfc}(-iz)$, where $\operatorname{erfc}(z)$ denotes the complementary error function. Screening by the electrons is of Yukawa-type, since the electron drift is negligible ($\mathbf{u}_e \ll v_{Te}$). The given dynamic dielectric function, Eq. (2), allows for an accurate representation of plasma screening, wakefield oscillations, ion and electron thermal effects, collisional and Landau damping [19, 21] and can be simply extended to include the effect of strong magnetic fields as well [22]. The streaming parameter (Mach number) for the classical case is expressed in terms of $M \equiv |\mathbf{u}_i|/c_s$, where $c_s \equiv \sqrt{k_B T_e / m_i}$ is the ion sound (Bohm) speed.

2.2 Quantum dielectric function

A quantum plasma of electrons is characterized by the degeneracy parameter $\theta = k_B T / E_F$, i.e. the ratio of the thermal energy ($\beta^{-1} = k_B T$) to the Fermi energy, as well as the Brueckner (or density) parameter $r_s = a/a_B$, defined as the ratio of the mean interparticle distance to the Bohr radius. For a quantum plasma of arbitrary degeneracy, the ideal dielectric function (random phase approximation) [23] reads

$$\epsilon_{\text{RPA}}(\mathbf{k}, \omega) = 1 + \frac{e^2}{\pi^2 k^2} \int d\mathbf{k}' \frac{f(\mathbf{k} + \mathbf{k}') - f(\mathbf{k}')}{\hbar\omega + i\delta - (E(\mathbf{k} + \mathbf{k}') - E(\mathbf{k}'))}, \quad (3)$$

where $E(\mathbf{k}) = \hbar^2 k^2 / 2m$ and $f(\mathbf{k}) = (1 + \exp[\beta(E(\mathbf{k}) - \mu)])^{-1}$ is the Fermi-Dirac function.¹ For the numerical evaluation, the dielectric function, Eq. (3), is separated into its real and imaginary part, for details see [24, 25]. Electronic collision effects are included in the dielectric description via the Mermin dielectric function [12, 26]

$$\epsilon_M(\mathbf{k}, \omega) = 1 + \frac{(\omega + i\nu)[\epsilon_{\text{RPA}}(\mathbf{k}, \omega + i\nu) - 1]}{\omega + i\nu[\epsilon_{\text{RPA}}(\mathbf{k}, \omega + i\nu) - 1] / [\epsilon_{\text{RPA}}(\mathbf{k}, 0) - 1]}, \quad (4)$$

which provides a (conserving) generalization in a static *relaxation time approximation* (RTA), where ν denotes the electron collision frequency. Hereafter, results for the quantum plasma are given in terms of the streaming parameter $M = u/v_F$ which is the ratio of the electrons' streaming velocity to the Fermi velocity.

2.3 QGP dielectric function

The linear response of a quark-gluon plasma to the passage of a fast parton with a velocity approaching the speed of light is described by following longitudinal dielectric function [14, 27]

$$\epsilon_{\text{QGP}}(k, \omega) = 1 + \frac{m_D^2}{k^2} \left(1 - \frac{\omega + i\nu}{2k} \ln \frac{\omega + i\nu + k}{\omega + i\nu - k} \right) \left(1 - \frac{i\nu}{2k} \ln \frac{\omega + i\nu + k}{\omega + i\nu - k} \right)^{-1}, \quad (5)$$

where collisions within the QGP are taken into account by a BGK collisional kernel with the momentum-independent collision rate ν . Furthermore, $m_D = gT(1 + n_f/6)^{1/2}$ is the Debye screening mass and n_f the number of quark flavors. For the QGP plasma the streaming parameter is defined as $M = u/c$, which is the ratio of the parton velocity in the QGP to the light speed.

¹ We note that the chemical potential μ explicitly depends on θ through the equation $\frac{2}{3}\theta^{-3/2} = \int_0^\infty \sqrt{x} / (1 + \exp(x - \beta\mu)) dx$.

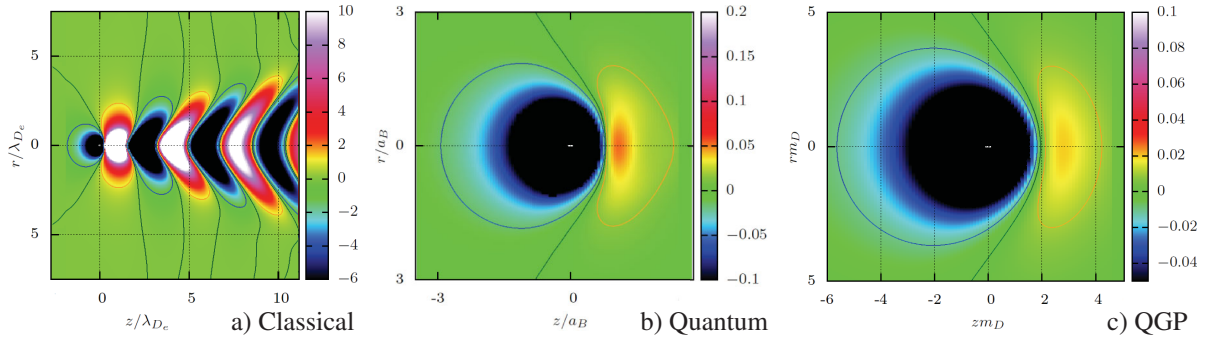


Fig. 1 Dynamically screened potentials for collisionless systems with $M = 0.55$: a) classical plasma with $T_e/T_i = 100$, b) quantum plasma with $\theta = 0.01$ and $r_s = 0.5$, c) QGP. Base units are mV , Hartree (a.u.), and $Q_a m_D$, respectively (for details see text). In the particle's frame of reference, the momentum vector is pointed from left to right along z -direction. For the sake of a comparable color scheme (of the trailing peak etc.), the potential values in the quantum plasma and QGP have been inverted (i.e., multiplied by -1). The result for the QGP agrees with Fig. 4 of [13].

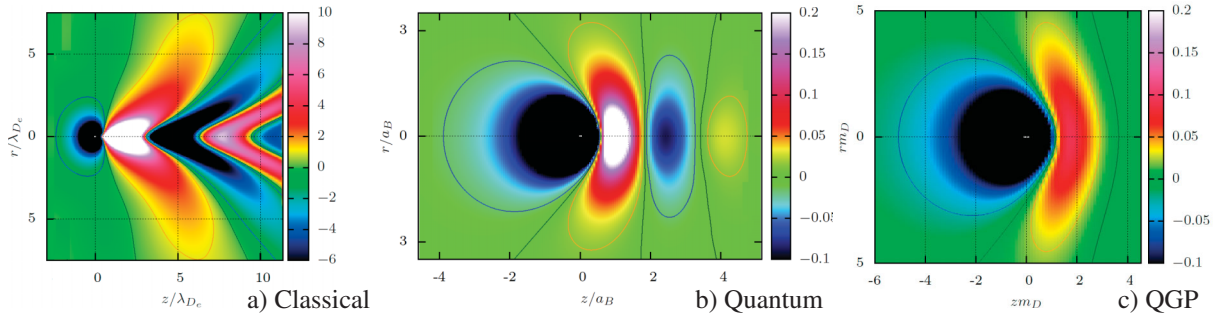


Fig. 2 Same as Fig.1 with $M = 0.99$. The result for the QGP agrees with Fig. 5 of [13].

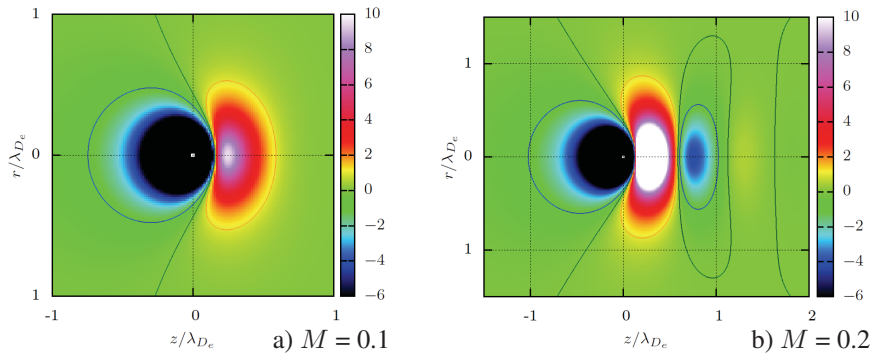


Fig. 3 DSP of the the classical plasma as in Fig.1 with a) $M = 0.1$, and b) $M = 0.2$.

3 Results

The topology of the DSPs of the considered classical, quantum and ultrarelativistic system are shown in Fig. 1 and Fig. 2 for two different values of the relevant streaming parameter, respectively. As the considered systems have different natural units, in the case of a classical plasma, the DSP is given in mV and in the case of the quantum plasma in Hartree atomic units. In the QGP the electric charges are replaced by color charges of quarks and gluons Q_a and the DSP is given in dimensionless units $\Phi/Q_a m_D$ [13].

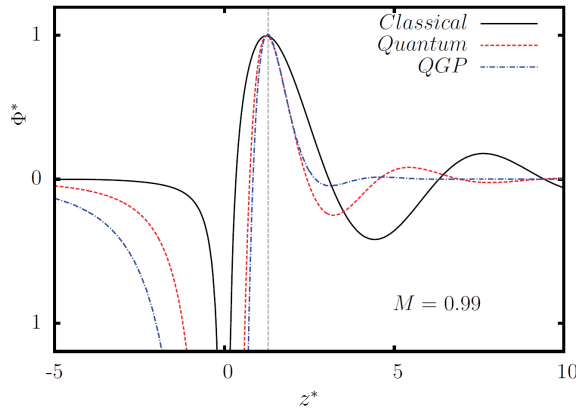


Fig. 4 Potential profile along the centre axis for $M = 0.99$. The potential values were scaled (and inverted, cf. Fig. 1) to match the DSPs at the position of their first peak $\Phi^*(z^* = 1) = 1$.

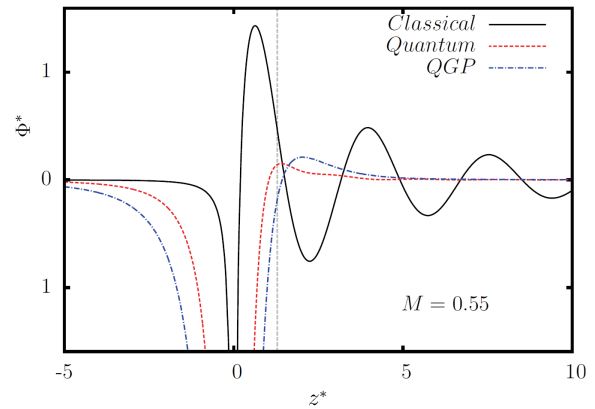


Fig. 5 Same as Fig. 4 but with $M = 0.55$ using identical scaling factors. The position of the first peak $z^* = 1$ for $M = 0.99$ is indicated by the light gray vertical line.

Let us start with the characteristics of the collisionless case. At a moderate (subsonic) streaming velocity $M = 0.55$, Fig. 1, all three DSPs exhibit substantial deviations from the static Yukawa potential with a distinct wakefield in backward direction of the particles' motion relative to the medium. The by far most pronounced potential anisotropy is found for the classical (dusty) plasma, Fig. 1a), where due to weak Landau damping ($T_e/T_i = 100$) even for a low Mach number a spatially extended oscillatory wake structure with several potential minima and maxima is present [18, 19]. In a quantum and color plasma, Figs. 1b), 1c), we note a quite similar shape of the wakefield, which in contrast to the classical case possesses only a single (attractive) trailing charged cloud with no alternating sign flips in the particle's wake. We note that the wakefield in Fig. 1b) is of pure quantum nature which disappears approaching the high temperature limit [25].

With increase of the streaming velocity to $M = 0.99$, Fig. 2, the classical wake forms a sharp Mach cone, while in the non-classical systems low-amplitude oscillations in the induced charged cloud trailing the fast particle are identifiable, cf. Fig. 4. The onset of oscillations in the wakefield behind a fast moving color charge akin to Čerenkov-like radiation was predicted for $M > 0.77$ [13]. In turn, for the appearance of an oscillatory wake potential in a quantum plasma (preluded by the appearance a second minimum), the (classical) kinetic drift energy of the streaming electron has to be larger than its quantum kinetic energy [25]. Interestingly, at reasonable (sufficiently high) values of the streaming parameter, the DSP in classical plasma has an apparent (Mach) cone-like V -shape, while the DSP around an ion (parton) in a quantum plasma (a QGP) reveals an inverse, forward bended V -shape [10, 11]. However, it is found that the classical potential exhibits at low values of the streaming parameter $M = 0.1, 0.2$ a rather similar topological structure as the DSP in quantum plasma or in the QGP, cf. Fig. 3a) with Fig. 1b), c) and Fig. 3b) with Fig. 2b), respectively.

The corresponding potential cuts along the center axis are shown for $M = 0.99$ in Fig. 4 and for $M = 0.55$, Fig. 5, respectively. In order to compare the topology and the characteristic scaling of the three physically completely different systems, we use as characteristic base unit of length the positions of the first potential peak and adjust the potential amplitudes to coincide at the first peak for $M = 0.99$, see Fig. 4. The same scaling is used in Fig. 5 for $M = 0.55$. In Fig. 4, it is found that the trailing potential peak has a very similar shape in both non-classical systems. In the QGP, the wakefield oscillations are, however, of very low amplitude. The classical potential has the most pronounced wakefield with the largest amplitude and oscillation wave length. The first peak is considerably more broadened than in the two other regimes. At a somewhat lower streaming velocity $M = 0.55$, Fig. 5, there is beside the repulsive short-range part only a very shallow attractive long-range potential part in the non-classical systems. The form of these wakes resembles the Lennard-Jones potential [13, 15, 28]. In contrast, the trailing potential peak in the classical case is even increased by 43 percent and the wakefield is revealing higher frequency oscillations compared to $M = 0.99$. In particular, we find that the DSPs show a completely different scaling behavior with the streaming parameter, cf. Figs. 4 and 5. While the classical wakefield reaches a maximum potential amplitude at a characteristic value $M_{cr} < 1$ [19] and flattens above M_{cr} , the amplitudes of the non-classical DSP are found to increase monotonically with the streaming velocity.

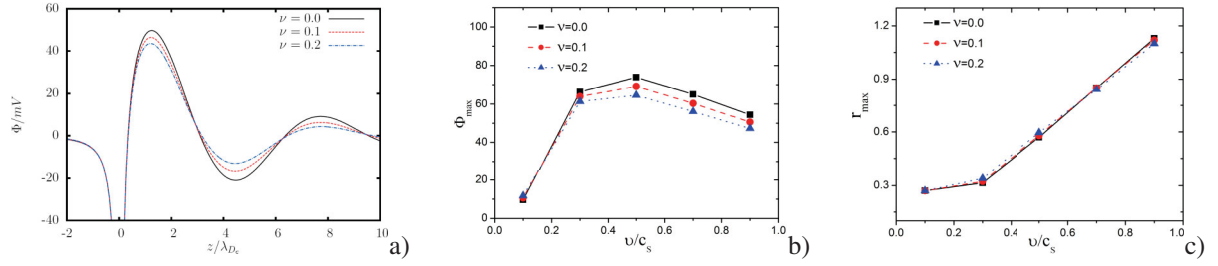


Fig. 6 Effect of collisions in a *classical plasma*: a) potential cut along the centre axis for different collision frequencies at $M = 1$, $T_e/T_i = 100$, b) absolute height and c) location of the potential maximum as function of drift speed.

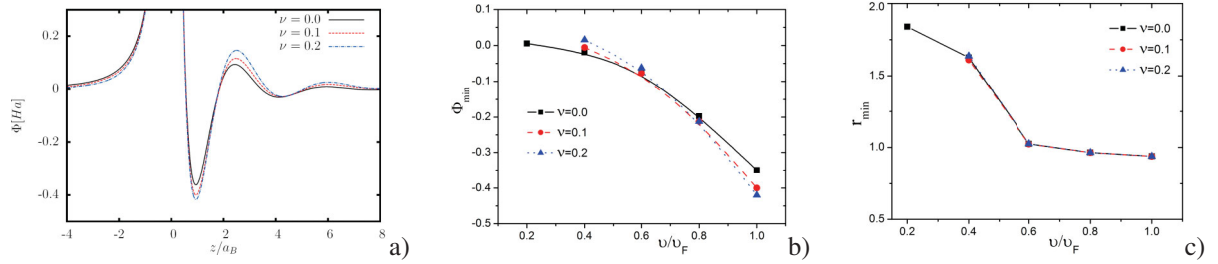


Fig. 7 Effect of collisions in a *quantum plasma*: a) potential cut along the centre axis for different collision frequencies at $M = 1$, $\theta = 0.01$, $r_s = 0.5$, b) absolute depth and c) location of the potential minimum as function of drift speed.

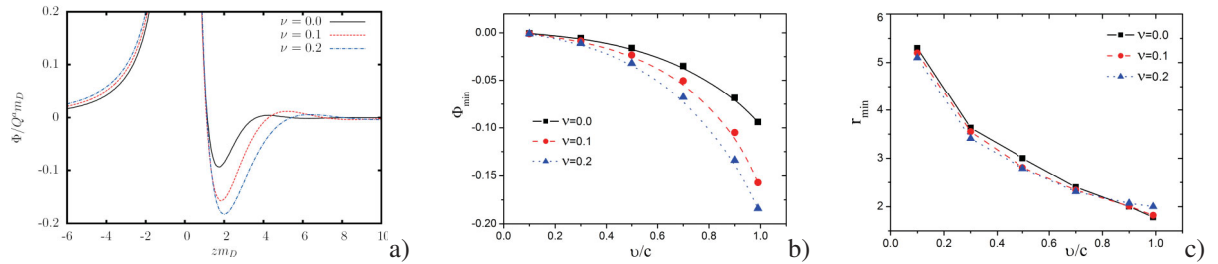


Fig. 8 Effect of collisions in a *ultrarelativistic plasma*: a) potential cut along the centre axis for different collision frequencies at $M = 0.99$, b) absolute depth and c) location of the potential minimum as function of drift speed.

A more detailed, systematic analysis of the parametrical scaling as function of the streaming velocity M and collisionality ν is presented in Figs. 6-8. We first consider results for the collisionless case plotted with a black solid line. Figure 6a) shows the potential profile of the classical DSP. With increasing in streaming velocity, Fig. 6b), the height of the trailing peak in the potential increases and reaches a maximum at M_{cr} . Above that value, the trend changes and the peak height is reduced with further increasing M [19]. A different behavior is found in the quantum plasma, Fig. 7, and the QGP, Fig. 8, as well. Here, the amplitude of the trailing potential minimum increases monotonically with the streaming parameter, not revealing a turning point in the considered regime $M < 1$. The position of the trailing peak in the wakefield as function of the streaming parameter is shown in Figs. 6c), 7c), and 8c), respectively. Classically, an increasing streaming velocity stretches the wakefield and shifts the trailing attractive potential peak away from the grain [19]. The opposite trend is observed for non-classical plasmas, where the trailing potential peak is shifted into closer vicinity of the perturbing particle, cf. Figs. 1, 2 and Figs. 4, 5. An in-depth analysis of the particular jump in the quantum regime is subject of ongoing work.

Finally, we consider the effect of finite collisions on the DSP, see red dashed line for $\nu = 0.1$ and dotted blue line for $\nu = 0.2$ in Figs. 6-8. Collisions are found to have only a insignificant effect on the position of the trailing potential peak. The strongest effect is observed for the QGP. Surprisingly, an increasing collision frequency leads to a strong *amplification* of the potential amplitude (the trailing potential minimum becomes

deeper), see Fig. 8(b). The finding that a finite collision rate can enhance the attractive and repulsive parts of the interaction potential behind a fast parton in a QGP was reported in [14] and recently confirmed [15]. Intuitively, interestingly, the potential amplitude should be damped (reduced) when finite collisions are taken in account as seen for the classical system, Fig. 6(b). Interestingly, also in the classical regime there is a slight anomalous wake amplification for $M = 0.1$. This collision-induced wake amplification is reproducible for $M < 0.2$ and is becoming even more pronounced for larger values of ν . Contrary to what one might suspect, this anomalous effect seems not to be an artefact of the linear response approximation as it is also present in PIC simulations, cf. curves for $M = 0.2$ (or $M = 0.3$) in Fig. 2(a) and (b) in Ref. [29]. In a quantum plasma, conventional collisional damping of the trailing potential peak is observed for $M \lesssim 0.65$. Above this value anomalous collisional damping (wake amplification) takes effect.

4 Conclusion

In this article, we present results for the dynamically screened potential in linear response approximation for classical, quantum and ultrarelativistic streaming plasmas. The dependence of the characteristic wake structure on the streaming velocity and collisionality of the plasmas is explored. The wake structure of a charged particle is most pronounced in a classical gas discharge plasma. The considered non-classical plasmas share several features with respect to the topology of their wakefield and its parametrical scaling. Collision-induced wake amplification is reported for all three systems. For an in-depth investigation of wake effects in quantum plasmas taking into account finite temperature and collision effects we refer to reference [25].

Acknowledgements This work has been supported by the Deutsche Forschungsgemeinschaft via grant SFB-TR24 Teilprojekt A9 and the Ministry of Education and Science of Kazakhstan under Grant No. 1415/GF2 2014 (IPC-21).

References

- [1] V.N. Tsytovich, G.E. Morfill, S.V. Vladimirov, and H.M. Thomas, “Elementary Physics of Complex Plasmas”, Lect. Notes Phys. **731**, Springer (2008).
- [2] T.S. Ramazanov, K.N. Dzhumagulova, A.N. Jumabekov, and M.K. Dosbolayev, Phys. Plasmas **15**, 053704 (2008).
- [3] M. Bonitz, C. Henning, and D. Block, Rep. Prog. Phys. **73**, 066501 (2010).
- [4] M. Bonitz, K. Becker, J. Lopez and H. Thomsen [eds.], “Complex Plasmas: Scientific Challenges and Technological Opportunities”, Springer Series on Atomic, Optical and Plasma Physics **59**, Springer (2014).
- [5] F.R. Graziani et al., High Energy Density Phys. **8**, 105 (2012).
- [6] P.M. Echenique, F. Flores, and R.H. Ritchie, Solid State Physics **43**, 229 (1990).
- [7] V. Malka et al., Science **298**, 1596 (2002).
- [8] M.D. Barriga-Carrasco, Laser Part. Beams **28**, 307 (2010).
- [9] D. Casas, M.D. Barriga-Carrasco, A.A. Andreev, M. Schnürer, and R. Morales, Acta Polytechnica, in press; arXiv:1409.6152 (2014).
- [10] D. Else, R. Kompaneets, and S.V. Vladimirov, Phys. Rev. E **82**, 026410 (2010).
- [11] D. Else, R. Kompaneets, and S.V. Vladimirov, EPL **94**, 35001 (2011).
- [12] P. Ludwig, M. Bonitz, and H. Kählert, J. Phys.: Conf. Series **220**, 012003 (2010).
- [13] P. Chakraborty, M.G. Mustafa, and M.H. Thoma, Phys. Rev. D **74**, 094002 (2006).
- [14] P. Chakraborty, M.G. Mustafa, R. Ray, and M.H. Thoma, J. Phys. G: Nucl. Part. Phys. **34**, 2141 (2007).
- [15] M. Mandal and P. Roy, Phys. Rev. D **88**, 074013 (2013).
- [16] V.S. Filinov, Yu.B. Ivanov, V.E. Fortov, M. Bonitz, and P.R. Levashov, Phys. Rev. C **87**, 035207 (2013).
- [17] V.S. Filinov, M. Bonitz, Yu.B. Ivanov, M. Ilgenfritz, and V.E. Fortov, accepted for publication in Contrib. Plasma Phys.; arXiv:1408.5714 (2014).
- [18] P. Ludwig, C. Arran, and M. Bonitz, “Introduction to Streaming Complex Plasmas B: Theoretical Description of Wake Effects” (in ref. [4]), pp 73-99 (2014).
- [19] P. Ludwig, W.J. Miloch, H. Kählert, and M. Bonitz, New Journal of Physics **14**, 053016 (2012).
- [20] P. Ludwig, H. Kählert, and M. Bonitz, Plas. Phys. Control. Fusion **54**, 045011 (2012).
- [21] M. Lampe, G. Joyce, and G. Ganguli, IEEE Trans. Plasma Science **33**, 57 (2005).
- [22] J.-P. Joost, P. Ludwig, H. Kählert, C. Arran, and M. Bonitz, Plasma Phys. Control. Fusion **57**, 025004 (2015).
- [23] J. Lindhard, Mat. Fys. Medd. Dan Vid. Selsk. **28**, 8 (1954).
- [24] N.R. Arista and W. Brandt, Phys. Rev. A **29**, 1471 (1984).
- [25] Zh. Moldabekov, P. Ludwig, M. Bonitz, and T. Ramazanov, The ion potential in warm dense matter: wake effects due to streaming degenerate electrons, submitted for publication; arXiv:1409.8079 (2014).
- [26] N.D. Mermin, Phys. Rev. B **1**, 2362 (1970).
- [27] M.E. Carrington, T. Fugleberg, D. Pickering, and M.H. Thoma, Can. J. Phys. **82**, 671 (2004).
- [28] B. Jiang and J. Li, Nuclear Physics A **856**, 121 (2011).
- [29] I.H. Hutchinson, Phys. Rev. E **85**, 066409 (2012).